



# Response of a grassland species to dry environmental conditions from water stable isotopic monitoring: no evident shift in root water uptake to wetter soil layers

Paulina Alejandra Deseano Diaz · Dagmar van Dusschoten · Angelika Kübert · Nicolas Brüggemann · Mathieu Javaux · Steffen Merz · Jan Vanderborght · Harry Vereecken · Maren Dubbert · Yuri Rothfuss

Received: 11 March 2022 / Accepted: 8 September 2022 / Published online: 21 September 2022  
© The Author(s) 2022

## Abstract

**Aims** We aimed at assessing the influence of above- and below-ground environmental conditions over the performance of *Centaurea jacea* L., a drought-resistant grassland forb species.

**Methods** Transpiration rate, CO<sub>2</sub> assimilation rate, leaf water potential, instantaneous and intrinsic water use efficiency, temperature, relative humidity, vapor pressure deficit and soil water content in one plant and root length density in four plants, all grown in custom-made columns, were monitored daily for 87 days in the lab. The soil water isotopic composition in

eleven depths was recorded daily in a non-destructive manner. The isotopic composition of plant transpiration was inferred from gas chamber measurements. Vertical isotopic gradients in the soil column were created by adding labeled water. Daily root water uptake (RWU) profiles were computed using the multi-source mixing model Stable Isotope Analysis in R (Parnell et al. PLoS ONE 5(3):1–5, 2010).

**Results** RWU occurred mainly in soil layer 0–15 cm, ranging from 79 to 44%, even when water was more easily available in deeper layers. In wet soil, the transpiration rate was driven mainly by vapor pressure deficit and light intensity. Once soil water content was less than 0.12 cm<sup>3</sup> cm<sup>-3</sup>, the computed canopy conductance declined, which restricted leaf gas exchange. Leaf water potential dropped steeply

---

Responsible Editor: Rafael S. Oliveira.

**Supplementary Information** The online version contains supplementary material available at <https://doi.org/10.1007/s11104-022-05703-y>.

---

P. A. Deseano Diaz · N. Brüggemann · M. Javaux · J. Vanderborght · H. Vereecken · Y. Rothfuss (✉)  
Institute of Bio- and Geosciences, Agrosphere (IBG-3),  
Forschungszentrum Jülich GmbH, Leo-Brandt-Straße,  
52425 Jülich, Germany  
e-mail: y.rothfuss@fz-juelich.de

D. van Dusschoten  
Institute of Bio- and Geosciences, Plant Sciences (IBG-2),  
Forschungszentrum Jülich GmbH, Leo-Brandt-Straße,  
52425 Jülich, Germany

A. Kübert  
Ökosystemphysiologie, Institut für Forstwissenschaften,  
Albert-Ludwigs-Universität Freiburg, 79110 Freiburg,  
Germany

M. Javaux  
Earth and Life Institute, Environmental Sciences  
(ELIE), Université catholique de Louvain (UCL),  
1348 Louvain-la-Neuve, Belgium

S. Merz  
Institute of Energy and Climate Research, Fundamental  
Electrochemistry (IEK-9), Forschungszentrum Jülich  
GmbH, Leo-Brandt-Straße, 52425 Jülich, Germany

M. Dubbert  
Leibniz-Institut für Agrarlandschaftsforschung  
ZALF Gewässerökologie und Binnenfischerei Berlin,  
Isotopebiogeochemistry and Gasfluxes, Müncheberg,  
Germany

to around  $-3$  MPa after soil water content was below  $0.10 \text{ cm}^3 \text{ cm}^{-3}$ .

**Conclusion** Our comprehensive data set contributes to a better understanding of the effects of drought on a grassland species and the limits of its acclimation in dry conditions.

**Keywords** Root water uptake · Water stable isotopes · Drought · *Centaurea jacea* · Non-destructive monitoring

## Introduction

In recent years, some researchers aim at investigating the strategies and mechanisms plants use to cope with dry soils and high temperatures from an ecohydrological perspective. That is, understanding the dynamic relationship between hydrological and biogeochemical processes within the plant community and between soil and vegetation (e.g., Newman et al. 2006; Dubbert et al. 2014; Chitra-Tarak et al. 2021) and how these links are impacted by climate change. Grasslands are a popular subject in ecohydrological studies due to the marked dependency of biological processes to changes in hydro-climatic conditions in these ecosystems (Zwicke et al. 2015; Yang et al. 2016) and their rapid response to these changes by setting in motion ecosystem-regulating processes (Jentsch et al. 2011). *Centaurea jacea* L. (brown knapweed), an ubiquitous forb native to grasslands, meadows and open well-lit spaces in Europe, North Asia and Northwest Africa (Hegi 1954) is well adapted to dry conditions and therefore a feasible study species for getting a mechanistic understanding of the feedbacks in the soil-plant-atmosphere continuum in a water-scarce environment.

The difference between water potential in the soil and in the surrounding environment drives root water uptake (RWU) and the magnitude of this difference depends on the rate of plant transpiration (Carminati and Javaux 2020). Plants actively control transpiration rate by opening or closing the stomata to “limit the variation in plant water potential with soil moisture and evaporative demand” (Sperry et al. 2002). It is an established belief that plant species in drying soil either set a relatively high leaf water potential limit by an “early” closing of the stomata (i.e., isohydricity) or display a

less strict stomatal control and much lower leaf water potential values (i.e., anisohydricity) (Tardieu and Simonneau 1998; Maseda and Fernández 2006). The magnitude and timing of stomata closure is pivotal, because through this process plants avoid hydraulic failure (i.e., xylem embolism), but it also causes the reduction of photosynthetic activity (Cowan and Farquhar 1977).

Evaluating stomatal control and quantifying RWU assist in the assessment of the role of water and nutrient availability, root distribution, radiation, temperature, relative humidity, among other factors, in the response of plants to dry conditions. Because many of these factors vary constantly in time and space, both stomatal control and RWU are highly dynamic processes. A single plant species might display iso- or anisohydric behavior depending on the environmental conditions and describing water uptake patterns might be challenging (Rothfuss and Javaux 2017), when relying on destructive sampling of soil and plant material at low spatio-temporal resolution. Non-destructive water stable isotopic monitoring coupled with laser-based spectroscopy has shown its potential in helping to overcome this challenge. In this method, the isotopic composition of soil water - that is, the relative ratio between the least abundant,  $^2\text{H}$  and  $^{18}\text{O}$ , and most abundant isotopes,  $^1\text{H}$  and  $^{16}\text{O}$ , i.e.  $\delta^2\text{H}$  and  $\delta^{18}\text{O}$ , expressed in per mil (‰), is computed from the measured isotopic composition of sampled water vapor. This method can be used in saturated and unsaturated soils in both the lab and the field at different depths of the soil profile (Rothfuss et al. 2013; Quade et al. 2018).

According to Rothfuss and Javaux (2017), several methods exist to quantify RWU using the isotopic composition of different soil layers or depths (“sources”) and the isotopic composition of plant transpiration (“product”). Multi-source (MS) mixing models with a Bayesian statistical approach do seem to outperform the graphical inference method and the two-end-member mixing model (Rothfuss and Javaux 2017). The most popular MS mixing model embedded in a Bayesian framework is the one developed by Parnell et al. (2010). The authors developed the Stable Isotope Analysis with R (SIAR) for dietary source partitioning, but it has proven quite suitable for RWU quantification (e.g., Prechsl et al. 2015; Volkmann et al. 2016; Beyer et al. 2018). This tool coupled with non-destructive isotopic monitoring allows the

calculation of RWU profiles with a 1-cm spatial and daily temporal resolution.

Since RWU is a process that depends on both above- and below-ground processes, it is essential to obtain comprehensive data sets in which both environmental and plant-related variables are simultaneously monitored. Comparing the evolution of these two types of variables can help in understanding the role of soil and leaf water status, and of root distribution on RWU, especially during drought. Moreover, this comparison can also help in describing the direction and magnitude of the feedbacks between environmental demand and soil water status, and stomatal conductance and leaf gas exchange. Therefore, our main purpose was to assess the performance of the drought-resistant grassland species *Centaurea jacea* under varying above- and below-ground environmental conditions. More specifically, we aimed at (i) linking leaf water status (i.e., leaf water potential) and gas exchange (i.e., CO<sub>2</sub> assimilation rate, canopy conductance, transpiration rate) with changes in environmental conditions (i.e., vapor pressure deficit and soil water content) and (ii) describe the role of root length density in RWU in both wet and dry environmental conditions in the soil and the atmosphere.

## Materials and methods

In the following subsections, our experimental set up is described in detail (a schematic view is presented in Fig. 1), as well as the measurement sequences and calculations used to determine and monitor above- and below-ground conditions and plant physiological variables. All calculations were done using the software R (R Core Team 2020).

### Soil columns and soil water isotopic measurements

Three columns made of polyvinyl chloride (PVC) and one acrylic column (11 cm diameter, 60 cm length, 5.7 l volume) were filled with loamy sand (standard soil 2.1, particle size distribution: 84.7% 2–0.063 mm, 11.4% 0.063–0.002 mm, 3.9% < 0.002 mm; LUFA Speyer, Germany) from which the largest ferromagnetic particles were removed. This was done in a semi-automated custom-made system, in which the soil is spread in a thin layer and passes under a set of rare earth magnets (NdFeB, 9×4×1 cm<sup>3</sup> size) on a conveyor belt (van

Dusschoten et al. 2016). The removal of large ferromagnetic particles is a critical step to avoid interferences in root observations with magnetic resonance imaging (MRI). The standard soil was used to be able to observe a higher percentage of roots measured with MRI in the PVC columns (referred to as “MRI columns” from this point onwards) (Pflugfelder et al. 2017). The dry bulk density was determined at 1.54 and 1.47 g cm<sup>-3</sup> for the MRI columns and acrylic column (referred to as “isotopic column” from this point onwards), respectively (Fig. 1).

The soil water vapor was sampled using the method described in Rothfuss et al. (2013) at eleven depths (1, 3, 5, 7, 10, 20, 40, 50, 53, 55 and 59 cm) in the isotopic column through a 17.5 cm-long gas-permeable polypropylene tubing (Accurel® PV8/2HF, 0.155 cm wall thickness, 0.55 cm i.d., 0.86 cm o.d., 0.2 μm pore size; 3 M, USA). Temperature was recorded at the aforementioned depths using thermocouples (type K, 0.01 °C precision; Greisinger electronic GmbH, Regenstauf, Germany). The volumetric soil water content ( $\theta$ , cm<sup>3</sup> cm<sup>-3</sup>) was recorded at depths of 1, 10, 50 and 59 cm with frequency domain sensors (EC-5, 0.001 m<sup>3</sup> m<sup>-3</sup> precision; Decagon Devices, USA) (according to Bogaen et al. (2007), the accuracy is lower, around 1–2% volume, when temperature, electric conductivity and supply voltage effects on the readings are taken into account). The  $\theta$  was recorded at depths 15, 25 and 34 cm with fixed capacitor sensors, similar to the ones used in the soil water profiler (SWaP, accuracy of 0.002 cm<sup>3</sup> cm<sup>-3</sup>) described in van Dusschoten et al. (2020). A calibration curve for each and one of the sensors was obtained at the same temperature, supply voltage and with the same soil used in our experiments by recording the sensors’ readings in soil with known volumetric water content.

The water vapor inside the tubing in each soil depth was sampled two times a day for 30 min with synthetic dry air (20.5% O<sub>2</sub> in N<sub>2</sub> with approximately 20–30 ppmV water vapor; Air Liquide, Germany) at low flow rate (approximately 70 ml min<sup>-1</sup>). The mixture of dry air and water vapor was carried to a Cavity Ring-Down Spectrometer (CRDS, L2130-i; Picarro, Santa Clara, USA) for online isotopic measurements. The mean soil water vapor isotopic composition ( $\delta^2\text{H}$  or  $\delta^{18}\text{O}$ ) value was calculated from the last 330 readings of the plateau (representing approximately the last 5 min and 30 s out of the 30 min of measurements). The corresponding liquid water  $\delta$ -value was

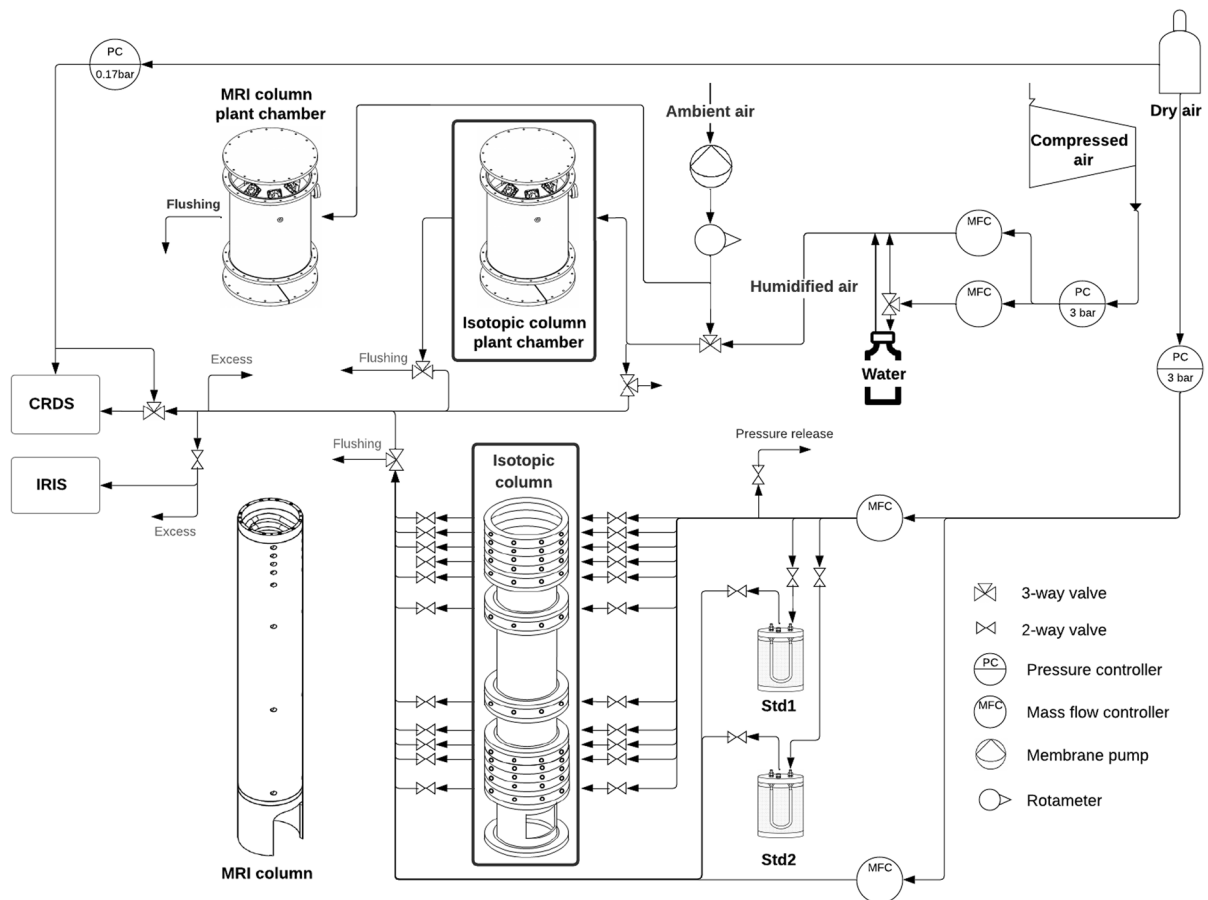


**Fig. 1** Piping and instrumentation diagram (PID) of the experimental setup placed in a climate chamber (temperature =  $19 \pm 0.22$  °C and relative humidity =  $64.7 \pm 1.3\%$ ): one isotopic column (framed by a black empty polygon), three magnetic resonance imaging (MRI) columns (only one is depicted next to the isotopic column) and a plant chamber over each column (a total of four, the isotopic column plant chamber framed by a black empty polygon and only one MRI column plant chamber are depicted). The relative humidity inside the isotopic column plant chamber was changed by increasing or decreasing the amount of water vapor saturated air from a water bottle mixed with compressed air (upper right section) entering the plant chamber. All soil water vapor isotopic meas-

calculated using the equations given by Majoube (1971) at the temperature measured at the observation depth, assuming a thermodynamic equilibrium between soil liquid water and water vapor. To account for the water vapor mixing ratio dependency of the CRDS measurements, the liquid water mean  $\delta$ -value was recomputed to a value of water vapor mixing ratio of 17,000 ppmV. Finally, this recomputed value was calibrated on the V-SMOW scale using two soil water vapor standards,

measurements were done online with a Cavity Ring-Down Spectrometer (CRDS) in the isotopic column and the rate and isotopic composition of plant transpiration was measured using the isotopic column plant chamber. The isotopic standards used were labeled Std1 and Std2.  $\text{CO}_2$  mixing ratio determinations in the isotopic column plant chamber were conducted with an Isotope Ratio Infrared Spectrometer (IRIS). The MRI columns were used to monitor root distribution on day after seeding (DaS) 237 and 307. The MRI columns and their respective plant chambers were not connected to the semi-automated water vapor sampling system and the MRI column plant chambers were flushed with air circulating in the climate chamber using a membrane pump and a rotameter

as described in Rothfuss et al. (2015) (Std1 and Std2 in Fig. 1). Each standard consisted of a smaller acrylic glass vessel filled with the same type of soil as the four columns containing a piece of gas-permeable tubing. The soil in one of the vessels was saturated with isotopically enriched water ( $\delta^2\text{H} = 102.4 \pm 1.4\text{‰}$  and  $\delta^{18}\text{O} = 30 \pm 0.3\text{‰}$ ), whereas the soil in the second vessel was saturated with isotopically depleted water ( $\delta^2\text{H} = -78.4 \pm 0.6\text{‰}$  and  $\delta^{18}\text{O} = -18.8 \pm 0.1\text{‰}$ ).

## Plant chamber and leaf measurements

A custom-made cylindrical plant chamber (29 cm diameter, 35.5 cm length, 23 l volume) was used to determine the isotopic composition and rate of plant transpiration and CO<sub>2</sub> assimilation of the plant growing in the isotopic column. The plants in the MRI columns were also enclosed each in a plant chamber with the same dimensions and were continuously flushed with ambient air using a membrane pump (Fig. 1). However, no isotopic or plant transpiration measurements were performed there. Each chamber was equipped with an air relative humidity (rh) and temperature (T) sensor (RFT-2, rh=2% and T=0.1 °C precision; METER Group, Munich, Germany) and enclosed a single plant individual. The soil surface of each column was covered with aluminum foil to avoid soil water evaporation. The air entering the plant chamber over the isotopic column (i.e., inlet airstream) was a mixture of ambient air and water vapor from a dew point generator (i.e., a water bottle equipped with an air diffuser, see Fig. 1). The outlet airstream from the plant chamber was a mixture of inlet airstream and plant transpiration. The inlet and outlet airstream were kept constant during each experimental period (Table 1) and were sampled six and three times per day for 31 min, respectively. The inlet airstream was sampled directly before and after each outlet airstream measurement. The isotopic composition and mixing ratio

of the water vapor in the inlet and outlet airstream were measured using the CRDS, and the mixing ratio of CO<sub>2</sub> was determined using an Isotope Ratio Infrared Spectrometer (IRIS, Delta Ray™; Thermo Scientific™, USA). These measurements were done five, eight and eleven hours after a fully programmable water-cooled LED panel (4×14 LED lamps à 20 W, 3200 K; Cree LED, USA) was switched on.

Leaf water potential ( $\Psi_l$ , MPa) of the plant in the isotopic column was monitored every 30 min using a psychrometer (PSY1, 0.1 MPa precision; Armidale, NWS, Australia). A broad leaf was selected and the surface over the midrib was carefully rubbed with sandpaper to expose the xylem. Afterwards, the leaf was rinsed with distilled water and the excess water was wiped. Then, the chamber of the psychrometer with greased edges was placed over the exposed midrib and fixed with a leaf clamp. The psychrometer was re-installed in this manner several times, because the leaf it was attached to had withered.

The vapor pressure deficit (vpd, kPa) inside the plant chamber was computed using Eq. (1) (Murray 1966).

$$vpd = \frac{100 - rh'}{100} 0.61078 e^{\frac{17.27 \times T_{leaf}}{T_{leaf} + 237.3}} \quad (1)$$

where  $T_{leaf}$  (°C) is the leaf temperature measured with the psychrometer and  $rh'$  (%) is the air relative humidity normalized to  $T_{leaf}$  calculated using Eq. (2).

**Table 1** Measured mean values of air temperature (T, °C) and relative humidity (rh, %) inside the isotopic column plant chamber, light intensity (mmol s<sup>-1</sup> m<sup>-2</sup>) and soil water content

Period (days after seeding - DaS)	T (°C)	rh (%)	vpd (kPa)	Light intensity (mmol s <sup>-1</sup> m <sup>-2</sup> )	$\theta$ (cm <sup>3</sup> cm <sup>-3</sup> )	Tr (mmol s <sup>-1</sup> m <sup>-2</sup> )
231–232	21.8±0.0	73.2±0.2	0.7±0.0	~500	0.22±0.01	3.5±0.1
234–235	21.8±0.1	65.9±1.7	0.9±0.0	~500	0.21±0.01	4.2±0.1
237–240	22.4±0.2	70.5±0.3	0.8±0.0	~500	0.21±0.02	2.8±0.4
243–248	22.5±0.1	62.7±1.4	1.0±0.0	~500	0.18±0.01	3.4±0.2
250–253	22.3±0.2	43.0±1.1	1.5±0.0	~500	0.15±0.01	4.1±0.3
256–267	22.4±0.2	67.1±0.6	0.9±0.0	~500	0.19±0.02	2.9±0.1
269–278 (HTr-I)	23.1±0.5	50±2.7	1.4±0.1	~1000	0.17±0.02	6.5±0.5
280–290 (HTr-II)	24.5±0.0	67.4±0.7	1±0.0	~1000	0.14±0.01	4.7±0.3
292–316 (LTr-I)	22.6±0.2	68.8±1.1	0.9±0.0	~500	0.17±0.03	2.9±0.1
318–323 (HTr-III)	24.4±0.1	42.4±2.2	1.8±0.1	~1000	0.10±0.02	4.7±0.5
325–327 (LTr-II)	22.7±0.0	50.3±2.5	1.4±0.1	~500	0.06±0.00	1.3±0.2

Values of vpd and Tr were calculated using Eqs. (1) and (3)

( $\theta$ , cm<sup>3</sup> cm<sup>-3</sup>), and computed values of vapor pressure deficit (vpd, kPa) inside the plant chamber and transpiration rate (Tr, mmol s<sup>-1</sup> m<sup>-2</sup>) for the different experimental periods

$$rh' = rh \left( \frac{P_{air}}{P_{leaf}} \right) \quad (2)$$

where  $rh$  (%) is the air relative humidity, and  $P_{air}$  and  $P_{leaf}$  are the vapor saturation pressure at the air and leaf temperature (kPa), respectively. The plant transpiration rate ( $Tr$ ,  $\text{mmol s}^{-1} \text{m}^{-2}$ ) was calculated using Eq. (3) (von Caemmerer and Farquhar 1981).

$$Tr = \frac{u_{in}(w_{out} - w_{in})}{s(1 - w_{out})} \quad (3)$$

where  $w_{in}$  (-) and  $w_{out}$  (-) are the mixing ratio of the water vapor in the inlet and outlet airstream of the plant chamber, respectively;  $u_{in}$  ( $\text{mmol s}^{-1}$ ) is the molar flow of air into the plant chamber and  $s$  ( $\text{m}^2$ ) is the soil surface area of the column ( $0.0095 \text{ m}^2$ ). The isotopic composition ( $\delta_{Tr}$ ) of plant transpiration was calculated using Eq. (4) (Dubbert et al. 2014).

$$\delta_{Tr} = \frac{w_{out}\delta_{out} - w_{in}\delta_{in}}{w_{out} - w_{in}} - \frac{w_{in}w_{out}(\delta_{out} - \delta_{in})}{w_{out} - w_{in}} \quad (4)$$

where  $\delta_{in}$  and  $\delta_{out}$  are the isotopic composition of the water vapor in the inlet and outlet airstream of the plant chamber, respectively. The  $\text{CO}_2$  assimilation rate ( $A$ ,  $\mu\text{mol s}^{-1} \text{m}^{-2}$ ) was calculated according to von Caemmerer and Farquhar (1981) (Eq. 5).

$$A = \frac{u_{in}}{s} \left[ c_{in} - c_{out} \frac{(1 - w_{in})}{(1 - w_{out})} \right] \quad (5)$$

where  $c_{in}$  (-) and  $c_{out}$  (-) are the  $\text{CO}_2$  mixing ratio in the inlet and outlet airstream of the plant chamber, respectively. The canopy conductance ( $G_s$ ,  $\text{mmol s}^{-1} \text{m}^{-2}$ ) was calculated using Eq. (6).

$$G_s = \frac{Tr}{vpd_l} \quad (6)$$

where  $vpd_l$  ( $\text{kPa kPa}^{-1}$ ) is the air-to-leaf  $vpd$  obtained dividing  $vpd$  by ambient pressure in kPa. The instantaneous and intrinsic water use efficiency ( $WUE$  and  $iWUE$ ,  $\mu\text{mol CO}_2 \text{ mmol}^{-1} \text{H}_2\text{O}$ , respectively) were calculated using Eqs. (7) and (8), respectively.

$$WUE = \frac{A}{Tr} \quad (7)$$

$$iWUE = \frac{A}{G_s} \quad (8)$$

Finally, the standard error in the calculation of  $Tr$  and  $A$  was computed using a first order Taylor series.

The average conditions inside the plant chamber are summarized in Table 1. The temperature inside the plant chamber was changed by (i) increasing or decreasing the light intensity of the LED panel and (ii) increasing or decreasing its vertical distance to the columns. The relative humidity was changed by increasing or decreasing the amount of vapor saturated air (from the dew-point generator) in the plant chamber's inlet airstream. The flow of air into the plant chamber ranged from  $4.3$  to  $11.9 \text{ l min}^{-1}$ .

### Isotopic labeling and drought experiment

The soil in the MRI and isotopic columns was saturated from the bottom with deionized tap water ( $\delta^2\text{H} = -51.6 \pm 0.6\text{‰}$  and  $\delta^{18}\text{O} = -7.7 \pm 0.1\text{‰}$ ) by applying a pressure head of around 1 m. Then, the columns were placed in a climate chamber ( $T = 19 \pm 0.22 \text{ °C}$  and  $rh = 64.7 \pm 1.3\%$ ) under the programmable water-cooled LED panel with a photoperiod of 14 h light and 10 h of darkness. The weight loss of the isotopic column was recorded (Plattformwaage DS, 0.2 g precision; Kern & Sohn GmbH, Germany) throughout the experiment to calculate the transpiration rate gravimetrically. *Centaurea jacea* was seeded shortly after saturation at a density of  $\sim 20$  seeds per  $95 \text{ cm}^2$ . On day after seeding 6 (DaS 6), the first seedlings were observed and on DaS 34, one individual was selected, while all other seedlings were removed.

The objective of our isotopic labeling strategy was (i) to create differences in isotopic composition among the potential soil water sources for plant transpiration in order to constrain the results of the mixing model, and (ii) to obtain complementary information from the  $\delta^2\text{H}$  and  $\delta^{18}\text{O}$  values by creating orthogonal profiles. The isotopic column was watered from the top using water low in  $\delta^2\text{H}$  and high in  $\delta^{18}\text{O}$  and from the bottom, using water high in  $\delta^2\text{H}$  and low in  $\delta^{18}\text{O}$  (Table S1) from DaS 256 to DaS 312. The plants in the MRI columns were watered using deionized tap water following the same protocol in terms of irrigation and timing. From DaS 313 to 327 no more water was added to the column in order to simulate a short drought period, during which

vpd was changed by changing rh inside the plant chamber as explained at the end of “[Plant chamber and leaf measurements](#)” section and by changing light intensity (Table 1).

### Root distribution measurements

Before (DaS 237) and towards the end (DaS 307) of the isotopic labeling period, the root system of the plants in the three MRI columns was monitored using a 4.7 T MRI magnet (Magnex, Oxford, UK). It was determined that roots with a diameter  $> \sim 0.3$  mm were visible. The root length in 2.5 cm-thick soil layers was obtained by processing the MRI images using the NMRrooting software according to van Dusschoten et al. (2016). At the end of the experiment (DaS 327), the roots of the isotopic column were harvested from the soil layers 0–2, 2–4, 4–6, 6–8, 8–11, 11–21, 21–41, 41–51, 51–54, 54–56, 56–58 and 58–60 cm and scanned (Expression 10000XL Model J181A; EPSON, Japan). The images were analyzed using the WinRhizo™ (Regent Instruments Inc., Quebec, Canada) software package for the determination of the total root length in each of the aforementioned soil layers. The root length density (RLD) in each soil layer in the MRI columns and in the isotopic column was calculated using Eq. (9)

$$RLD_z = \frac{RL_z}{V_z} \quad (9)$$

where  $RL_z$  (cm) is the total root length in soil layer  $z$  and  $V_z$  ( $\text{cm}^3$ ) is the soil volume of layer  $z$ .

Due to time and technical constraints, root distribution in the MRI columns was not measured with MRI at the end of the experiment (i.e., DaS 327), nor were the roots in these columns harvested and scanned. This decision did not limit the analysis of our results, since we did not aim at systematically comparing the scan and MRI methods.

### Calculation of RWU profiles

The relative contribution to plant RWU from the different soil layers was calculated at a daily resolution using the Bayesian statistical model SIAR (Parnell et al. 2010) using the  $\delta^2\text{H}$  and  $\delta^{18}\text{O}$  of the soil and plant transpiration. The function used inside the SIAR package, i.e. *siarmcmkdirichletv4*,

uses a Markov chain Monte Carlo algorithm to produce estimated proportions of the sources (i.e.,  $\delta_{\text{soil water}}$  in the different soil depths) in the observed mix or product (i.e.,  $\delta_{\text{Tr}}$ ). The used prior distribution for the sources' proportions in this function is the Dirichlet. The calculation of the sources' proportions or relative contributions of soil water at the eleven depths to plant transpiration from DaS 270 to 327 are detailed in Appendix 1. The absolute contribution of each soil layer or sink term ( $\text{cm}^3$  water  $\text{cm}^{-3}$  soil  $\text{day}^{-1}$ ) to plant transpiration (referred to as “RWU profile” from this point onwards) was calculated as the product of transpiration rate and the relative contribution for each analyzed day at each depth. This value is always positive and this is why RWU values in our study are a quantification of the amount of water flowing only from the soil via the roots to the leaves on a daily basis. However, we did not quantify the overall uptake by the roots at a certain depth, which includes also the water uptake that may be redistributed via the root system to other soil layers (i.e., root water redistribution).

Additionally, RWU daily profiles were calculated using only  $\delta^2\text{H}$  or  $\delta^{18}\text{O}$  values and they were statistically compared to the RWU profiles calculated with both  $\delta^2\text{H}$  and  $\delta^{18}\text{O}$  values. First, the Shapiro-Wilk normality test was applied to every profile and, according to the result; either a paired t-test or the non-parametric paired Wilcoxon-test was used to compare the RWU profiles. The analyzed periods were DaS 270 to 278, 280 to 290, 292 to 316, 318 to 323 and 325 to 327 referred to as HTr-I (high transpiration rate I), HTr-II, LTr-I (low transpiration rate I), HTr-III and LTr-II, respectively.

## Results

A brief summary of the evolution of measured and calculated variables is presented in the first subsection, followed by a description of the obtained isotopic profiles during and after the isotopic labeling. The series of calculations to obtain RLD profiles in the isotopic column and MRI columns is detailed in the third subsection. In the last subsection, we report on the observed RWU patterns of *Centaurea jacea*.

## Dynamics of environmental conditions and plant-related variables

The temporal variation of directly measured (air temperature -  $T_{air}$ ,  $T_{leaf}$ , rh,  $\Psi_l$ , and  $\theta$ ) and calculated variables (vpd, Tr, WUE, iWUE, A, and  $G_s$ ) are shown in Fig. 2. In Fig. 2a the temporal variation of daily mean  $T_{leaf}$ ,  $T_{air}$  and rh values are displayed.  $T_{leaf}$  was slightly higher than  $T_{air}$  in some periods (up to 0.8 °C). Tr dynamics was similar to the dynamics of vpd for most DaS (Fig. 2b), whereas A dynamics was similar to that of  $G_s$  (Fig. 2d). Note that  $G_s$ , Tr and A started dropping progressively to zero from DaS 319 onwards, a trend that will be discussed in depth in “Plant response to drought” section. Until DaS 322,  $\Psi_l$  was higher than -1.5 MPa and after this point, it decreased more markedly compared to previous periods: it decreased from -1.49 MPa to

-3.19 MPa during the last six days of the experiment (Fig. 2c). The WUE remained constant until the end of LTr-I (DaS 313), after which it decreased until around DaS 320 (mid-HTr-III) with an again constant period until the end of the experiment. On the other hand, iWUE values were constant during the experiment and even increased slightly during the last days (Fig. 2e). The water content of the bottom half of the isotopic column was higher compared to the water content of the top half until DaS 265. Afterwards,  $\theta$  became more homogeneous across the whole soil column, ranging from  $0.07 \pm 0.01$  to  $0.24 \pm 0.08 \text{ cm}^3 \text{ cm}^{-3}$  (Fig. 2f).

## Isotopic labeling

After the first labeling stage from DaS 270 to DaS 290 (Table S1), the differences in  $\delta_{\text{soil water}}$

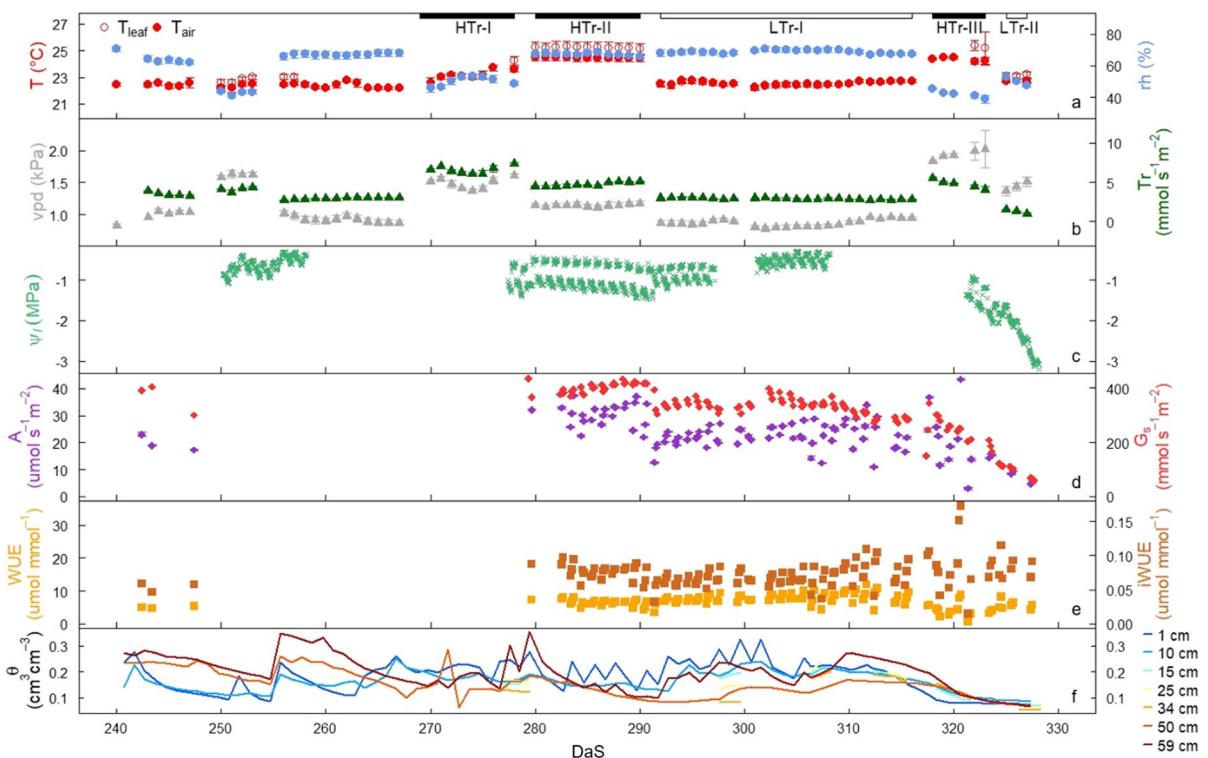


**Fig. 2** Time series (DaS: days after seeding) of the daily measured air temperature ( $T_{air}$ , °C), leaf temperature ( $T_{leaf}$ , °C) and relative humidity (rh, %) (a); of vapor pressure deficit (vpd, kPa) and transpiration rate calculated from the isotopic column plant chamber measurements (Tr,  $\text{mmol s}^{-1} \text{ m}^{-2}$ ) (b); of leaf water potential ( $\Psi_l$ , MPa) (c); of  $\text{CO}_2$  assimilation rate (A,  $\mu\text{mol s}^{-1} \text{ m}^{-2}$ ) and canopy conductance ( $G_s$ ,  $\text{mmol}$

$\text{s}^{-1} \text{ m}^{-2}$ ) (d); of instantaneous and intrinsic water use efficiency (WUE and iWUE,  $\mu\text{mol mmol}^{-1}$ ) (e); and of volumetric soil water content ( $\theta$ ,  $\text{cm}^3 \text{ cm}^{-3}$ ) at different soil depths (f). Filled black polygons mark the periods with high transpiration rate (HTr-I, HTr-II and HTr-III) and empty polygons, periods with low transpiration rate (LTr-I and LTr-II)

values among layers were considerable only in layer 7–50 cm (Fig. 3a). Increasing and decreasing the  $\delta$ -value of the added labeled water (labeling stage 2 and 3 in Table S1) resulted in a progressively steeper isotopic gradient in layer 7–50 cm (Fig. 3b and c), while a steep gradient in layer 50–60 cm was reached until labeling stage 3 (Fig. 3c). Nonetheless, the isotopic profile in layer 0–7 cm remained homogeneous from the beginning of the labeling until DaS 318. That is, no gradient was observed during the three labeling stages. After DaS 318, when no more water was added to the column, the isotopic gradient in layer 20–60 cm remained steep, whereas the isotopic profile in layer 0–10 cm evolved in a heterogeneous manner. The  $\delta^2\text{H}$  values at 1, 5 and 10 cm increased faster than those at 3 and 7 cm. Simultaneously, the  $\delta^{18}\text{O}$  values at 1, 5, and 10 cm decreased faster than those at 3 and 7 cm (Fig. 3d).

The highest and lowest  $\delta^2\text{H}$  values reached in the soil were  $216.4 \pm 0.7\text{‰}$  at depth 59 cm (DaS 312) and  $-69.9 \pm 0.6\text{‰}$  at depth 3 cm (DaS 313), respectively. The highest and lowest  $\delta^{18}\text{O}$  values were  $24.5 \pm 0.3\text{‰}$  at depth 3 cm (DaS 313) and  $-39.5 \pm 0.3\text{‰}$  at depth 59 cm (DaS 312), respectively. That is, the minimum  $\delta^2\text{H}$  and the maximum  $\delta^{18}\text{O}$  values in soil water at the top of the column were measured the last day where labeled water was added (i.e., DaS 312). The

maximum  $\delta^2\text{H}$  and the minimum  $\delta^{18}\text{O}$  values at the bottom were measured the following day (i.e., DaS 313). The  $\delta_{\text{soil water}}$  values at 59 cm depth, were very similar to the  $\delta$ -values of the labeled water added to the bottom ( $\delta^2\text{H} = 220\text{‰}$ ;  $\delta^{18}\text{O} = -40\text{‰}$ , stage 3 in Table S1). A larger difference between the  $\delta_{\text{soil water}}$  values at the top and the added labeled water ( $\delta^2\text{H} = -90\text{‰}$ ;  $\delta^{18}\text{O} = 29\text{‰}$ , stage 3 in Table S1) was found. Most daily  $\delta_{\text{Tr}}$  values plot over the  $\delta_{\text{soil water}}$  values from the upper 10 cm of the column (Fig. 4b). From around DaS 310 onwards, the  $\delta_{\text{Tr}}$  values progressively plot closer to the  $\delta_{\text{soil water}}$  values in deeper soil layers (Fig. 4a). Since the labeling water was only enriched with one of the isotopologues at a time,  $\delta^2\text{H}$  and  $\delta^{18}\text{O}$  were negatively correlated (Fig. 4).

### Root length distribution

The objective of the MRI measurements of the MRI columns on Das 237 and 307 was to non-destructively produce RLD profiles inside the isotopic column at these same dates. The comparison between the MRI pictures from the MRI columns and the scanning of the roots of the isotopic column at the end of the experiment (DaS 327) showed that root length measured with WinRhizo<sup>TM</sup> in the isotopic column was around ten times higher than root length measured

**Fig. 3** Temporal changes in soil water (circles) and plant transpiration (triangles)  $\delta^2\text{H}$  and  $\delta^{18}\text{O}$  values during the isotopic labeling stage 1 (a, day after seeding (DaS) 256–290), stage 2 (b, DaS 291–304) and stage 3 (c, DaS 305–312) and when the soil was drying (d, DaS 313–327)

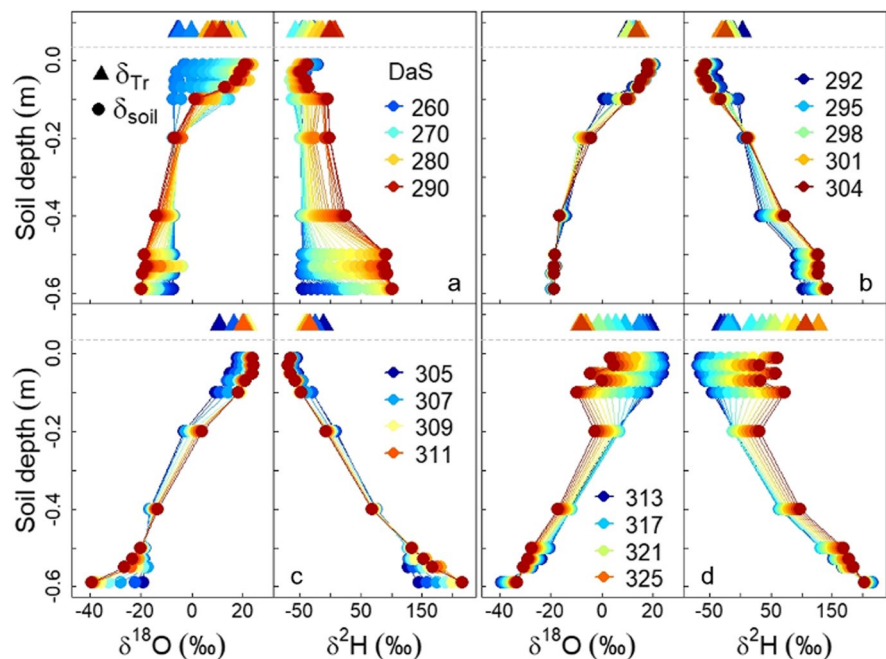
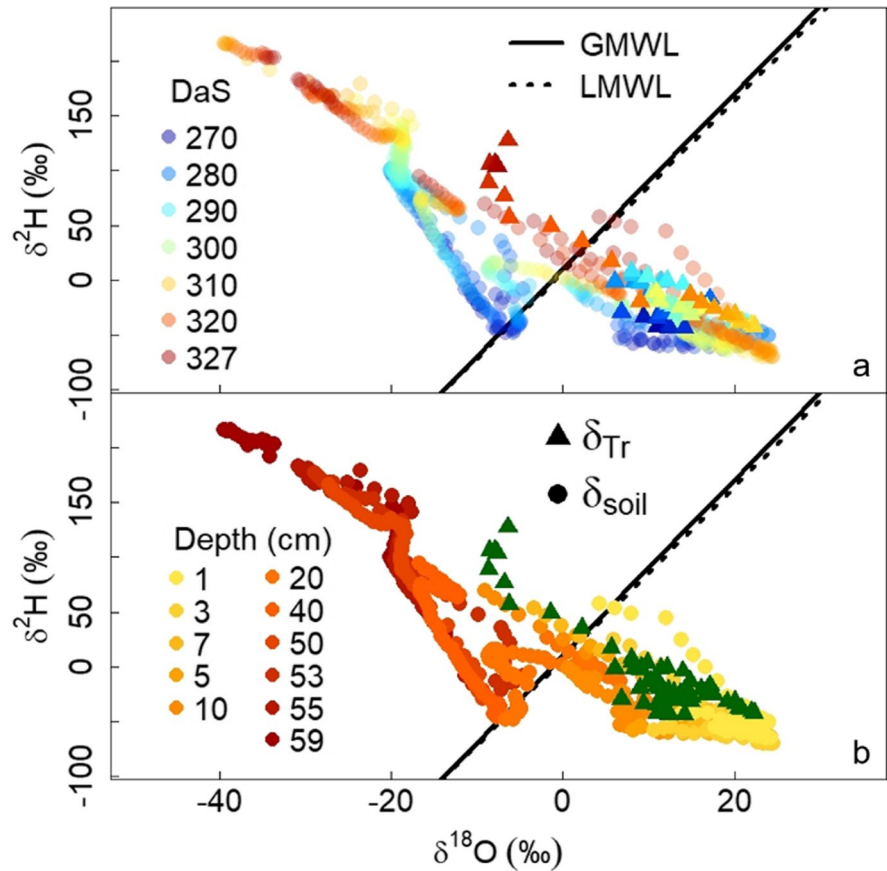


**Fig. 4** Temporal (a) and spatial (b) dynamics in the relationship between  $\delta^2\text{H}$  and  $\delta^{18}\text{O}$  in soil water (circles) and plant transpiration (triangles) from day after seeding (DaS) 270 to 327. The global (solid black line) and local (dotted black line) meteoric water lines (GMWL and LMWL, respectively) are included as a reference. In panel a, the temporal dynamics of plant transpiration and soil water  $\delta$ -values from DaS 270 to 327 are represented by a color scale from cold to warm tones. In panel b, the spatial dynamics of the soil water  $\delta$ -values in eleven soil depths from the top to the bottom are represented by a color scale from yellow to red



with MRI in the MRI columns (compare x-axis of Fig. 5a and b). In order to assess the magnitude of this discrepancy, a ratio was calculated for five soil horizons (0–10, 10–20, 20–40, 40–50 and 50–60 cm). This ratio was obtained by dividing the scan-derived RLD values measured on DaS 327 in the isotopic column by the MRI-derived RLD values measured on DaS 237 and DaS 307 (Table S2) in each MRI column. The mean of the ratios was  $10.8 \pm 2.9$  and no systematic differences across soil layers or columns were identified.

The maximum root length density on DaS 237, 307 and 327 was observed at depth 59 cm ( $3.0 \pm 2.6$  cm  $\text{cm}^{-3}$ ,  $3.7 \pm 3.1$  cm  $\text{cm}^{-3}$  and  $52.2$  cm  $\text{cm}^{-3}$ , respectively). In all profiles, RLD values in layers 0–10 cm and 50–60 cm were higher than the RLD values in the middle section of the column (i.e., layer 10–50 cm). The higher RLD values at depth 59 cm are most likely the product of pot-bound roots, which could be a consequence of the extended time the plants grew in the columns.

#### Daily RWU profiles

The RWU profiles obtained using both  $\delta^2\text{H}$  and  $\delta^{18}\text{O}$  input data (referred to as “ $\delta^2\text{H}$ - $\delta^{18}\text{O}$ -derived”) in days with high Tr (i.e., HTr-I, -II and -III) compared to days with low Tr (i.e., LTr-I and -II) were very similar (Fig. 6a). RWU was highest in layer 0–15 cm, second highest in layer 45–60 cm and lowest in the middle section of the column (i.e., 15–45 cm). In LTr-I and LTr-II, an average of  $79 \pm 4\%$  and  $44 \pm 4\%$  of the total RWU, respectively, was extracted in layer 0–15 cm, while  $13 \pm 4\%$  and  $44 \pm 4\%$  in the same respective periods was extracted in layer 45–60 cm. An average of  $69 \pm 5\%$  in HTr-I and HTr-II, and  $56 \pm 9\%$  in HTr-III of the total RWU was extracted in layer 0–15 cm, while around  $22 \pm 5\%$  in HTr-I and HTr-II and  $35 \pm 8\%$  in HTr-III was extracted in layer 45–60 cm. Note that during the last two periods (i.e., HTr-III and LTr-II), RWU in layer 0–15 cm was lower and in layer 45–60 cm was higher compared to RWU in the same soil layers in previous periods.

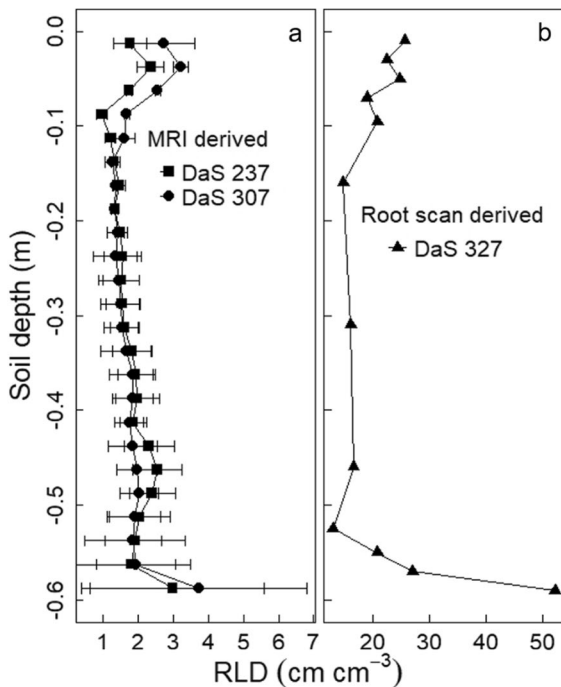


**Fig. 5** Mean root length density (RLD,  $\text{cm}^3 \text{root cm}^{-3} \text{soil}$ ) profile derived from the non-destructive magnetic resonance imaging (MRI) measurements on day after seeding (DaS) 237 (squares) and 307 (circles) in the MRI columns (a) and RLD derived from the destructive root scan measurement at the end of the experiment on DaS 327 in the isotopic column (b)

The RWU profiles obtained using either  $\delta^2\text{H}$  or  $\delta^{18}\text{O}$  input data (referred to as “ $\delta^2\text{H}$ -derived” and “ $\delta^{18}\text{O}$ -derived”, Fig. 6b and c, respectively) were not statistically different from the  $\delta^2\text{H}$ - $\delta^{18}\text{O}$ -derived RWU profiles (except between  $\delta^2\text{H}$ - and  $\delta^2\text{H}$ - $\delta^{18}\text{O}$ -derived profiles in DaS 245, Table S3). In general, the RWU in layer 0–15 cm and 45–60 cm in the  $\delta^2\text{H}$ - and  $\delta^{18}\text{O}$ -derived profiles was slightly lower than RWU in  $\delta^2\text{H}$ - $\delta^{18}\text{O}$ -derived profiles in the same layers. Consequently, RWU in layer 15–45 cm in the  $\delta^2\text{H}$ - and  $\delta^{18}\text{O}$ -derived profiles was slightly higher than RWU in the  $\delta^2\text{H}$ - $\delta^{18}\text{O}$ -derived profile (Fig. 6a-c).

As already mentioned in “Dynamics of environmental conditions and plant-related variables” section,  $\theta$  was rather homogeneous along the column from DaS 265 onwards, that is, for all days where RWU profiles were calculated. However, some differences in the water saturation between soil layers are visible in Fig. 6d. For example, there was consistently less water in layer 30–55 cm than in the rest of the

layers from around DaS 285 until around DaS 307. Afterwards, the  $\theta$  profile was more homogeneous with a decreasing trend. Due to our labeling strategy, soil layers 0–5 cm and 55–60 cm were wetter than the rest of the layers from DaS 270 to DaS 312.

Daily changes in RWU profiles did not match those of  $\theta$  for some periods. In LTr-I, the RWU was higher in layer 0–20 cm than deeper in the soil profile (Fig. 7a). However,  $\theta$  in this layer did not decrease much faster than deeper in the soil profile (Fig. 7b). In HTr-III,  $\theta$  in layer 10–60 cm decreased slightly faster than in layer 0–10 cm (Fig. 7d), even though the RWU in layer 0–10 cm was higher than in the rest of the column (Fig. 7c).

## Discussion

In the first two subsections, we describe the response of *Centaurea jacea* to dry conditions through correlations of the environmental and plant-related variables and a simple hydraulic model. In the last subsection, we link RWU changes of *C. jacea* and the dynamics of above- and below-ground environmental conditions and root distribution. We observed a stricter control of the stomata by *C. jacea* when vpd was high and the soil was drying. The increasingly dry soil seemed to set off stomatal closure. Under varying hydro-climatic conditions, most of the water extracted by *C. jacea* came from the soil layer 0–15 cm (up to 79%) and the second greatest contribution (up to 44%) came from the soil layer 45–60 cm. In most days, water availability and root distribution seemed to be the main drivers of RWU.

### Plant response to drought

The statistically significant correlations between measured and calculated variables are displayed in Fig. 8. In general, we interpret changes in the correlations between canopy conductance,  $G_s$ ; transpiration rate,  $\text{Tr}$ ; vapor pressure deficit, vpd; and soil water content,  $\theta$ , as a stricter control over transpiration rate by *Centaurea jacea* through stomatal closure when both above- and below-ground conditions were dry. Before DaS 319, the relationships between  $\theta$  and  $\text{Tr}$ , and between  $\theta$  and  $G_s$  were not unique (i.e., there were several  $\text{Tr}$  or  $G_s$  values for

**Fig. 6** Temporal changes in the sink term profiles ( $\text{cm}^3 \text{ water cm}^{-3} \text{ soil day}^{-1}$ ) in the isotopic column calculated with both soil water  $\delta^2\text{H}$  and  $\delta^{18}\text{O}$  profiles (a,  $\delta^2\text{H}$ - $\delta^{18}\text{O}$ -derived), with  $\delta^2\text{H}$  profiles only (b,  $\delta^2\text{H}$ -derived) and with  $\delta^{18}\text{O}$  profiles only (c,  $\delta^{18}\text{O}$ -derived) during isotopic labeling and until the end of the experiment. The temporal changes in volumetric soil water content profiles ( $\theta$ ,  $\text{cm}^3 \text{ cm}^{-3}$ ) during the experiment is shown in panel d. Filled black polygons mark the periods with high transpiration rate (HTr-I, HTr-II and HTr-III) and empty polygons, periods with low transpiration rate (LTr-I and LTr-II). The gray downward arrows represent water added to the top of the column and the upward gray arrows, water added to the bottom. Thicker arrows represent a higher amount of water added

one single  $\theta$  value) and seemed to depend on vpd (empty circles in Fig. 8c and e, respectively). After DaS 319, both  $G_s$  and Tr decreased markedly with small changes in  $\theta$  (filled circles in Fig. 8c and e, respectively). Interestingly, both  $\text{CO}_2$  assimilation rate, A; and Tr were positively correlated to  $G_s$  (Fig. 8d and f, respectively). However, only the correlation between  $G_s$  and Tr changed with vpd: the higher the vpd, the higher the slope (0.002 for  $\text{vpd} < 1 \text{ kPa}$ , 0.01 for  $1 < \text{vpd} < 1.5 \text{ kPa}$  and 0.02 for  $\text{vpd} > 1.5 \text{ kPa}$  in Fig. 8f). We also observed a different and significant correlation between vpd and Tr when comparing the data before DaS 319 (slope = 4.14,  $r^2 = 0.68$ , p-value =  $2.2 \times 10^{-16}$ ) and after DaS 319 (slope = 5.87,  $r^2 = 0.86$ , p-value =  $6.2 \times 10^{-4}$ ).

Through stomatal closure in dry conditions, *C. jacea* displayed a slightly more efficient water use in laboratory conditions. We observed a slight increase in intrinsic water use efficiency, iWUE and a constant instantaneous water use efficiency, WUE (Fig. 1e). Similarly, Kübert et al. (2021) observed an increase in iWUE and no change or a small decline in WUE of *C. jacea* in dry conditions in the field. In our experiment, WUE and vpd were significantly and negatively correlated (slope = -3.70,  $r^2 = 0.63$ , p-value =  $1.2 \times 10^{-9}$ ) during the drought period. Yet, several studies reported higher WUE values in grassland species during drought (e.g., Judson et al. 2006; Gang et al. 2016; Yue et al. 2020). These contradictory outcomes could be attributed to differences in temporal and spatial scales: the studies of Gang et al. (2016) and Yue et al. (2020) encompassed data at a global scale and from several years. Alternatively, they could be attributed to the fact that, in the experiments

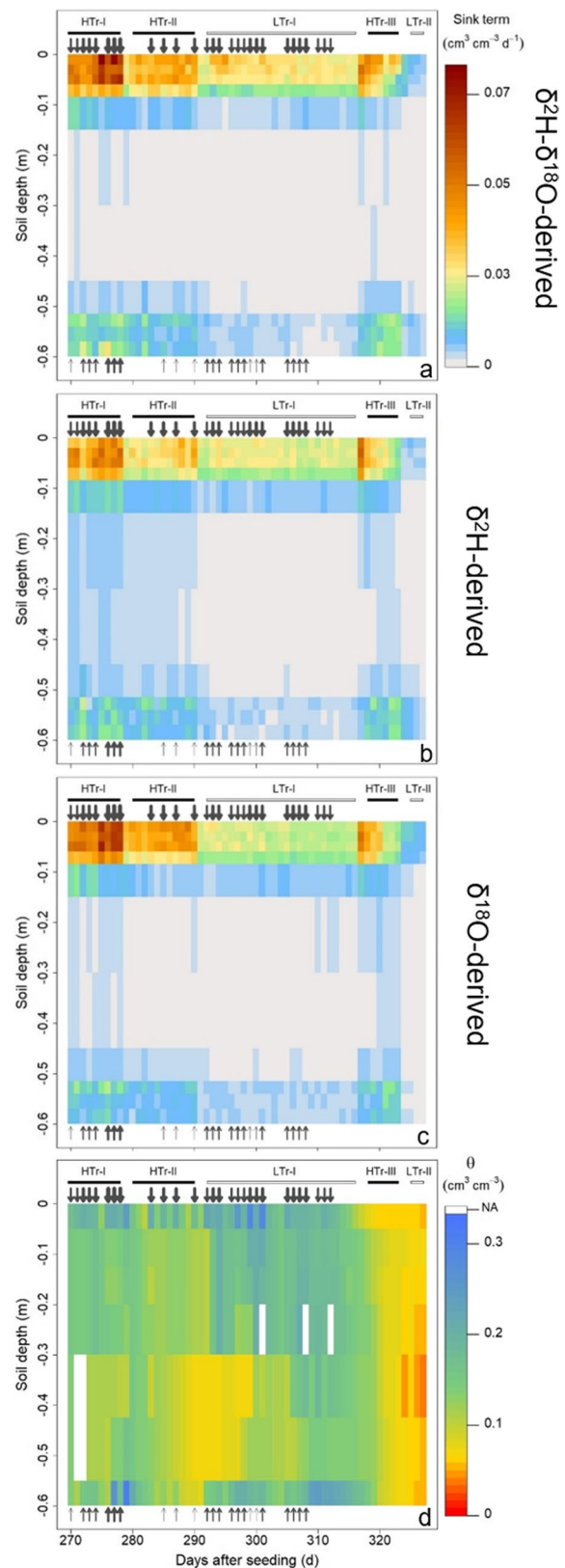
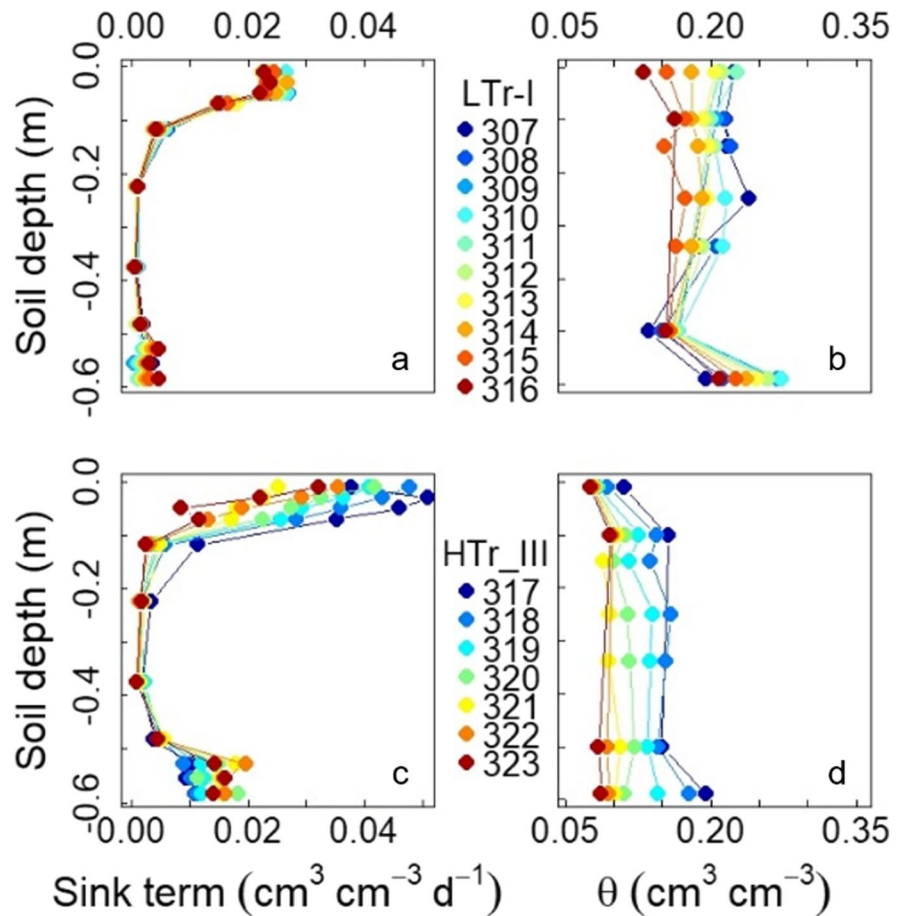


**Fig. 7** Temporal changes in the sink term ( $\text{cm}^3 \text{ water cm}^{-3} \text{ soil day}^{-1}$ ) (a) and in volumetric soil water content profiles ( $\theta$ ,  $\text{cm}^3 \text{ cm}^{-3}$ ) (b) during period of low transpiration rate I (LTr-I) and during period of high transpiration rate III (HTr-III) in the isotopic column



conducted by Kübert et al. (2021) and in this study, lower  $\theta$  ( $<0.1 \text{ cm}^3 \text{ cm}^{-3}$ ) and higher vpd ( $>1 \text{ kPa}$ ) values were observed than those reported by Judson et al. (2006).

According to Sperry and Love (2015), water flux from the soil to the leaves can be mathematically described by a “supply function”, in which Tr is expressed as a function of canopy xylem pressure ( $P_{\text{canopy}}$ ) at constant  $\theta$ . The slope of the relationship (also referred to as soil-canopy conductance by the authors) is positive and relatively linear at high xylem pressure (i.e., close to zero) and low to medium Tr, and decreases with decreasing xylem pressure (i.e., more negative) and increasing Tr. The slope approaches zero at high Tr and low  $P_{\text{canopy}}$ , while Tr approaches a constant maximum value referred to as a critical Tr value (associated with a critical  $P_{\text{canopy}}$  value) after which hydraulic failure takes place. In drier soils, the

Tr( $P_{\text{canopy}}$ ) relationship is “flatter” than in wet soils and therefore, the critical Tr value is lower than in wetter soils. The authors argue that through stomatal closure the plants avoid reaching the critical Tr and  $P_{\text{canopy}}$  values, especially when vpd is high and the soil is dry. We hypothesize that the drop in  $G_s$  in our experiment observed at DaS 319 might have occurred to counteract the effect of high vpd and low  $\theta$ . In other words, to avoid approaching a theoretical non-linear region of the relationship between Tr and leaf water potential,  $\Psi_l$  (i.e., slope  $\approx 0$  at higher Tr and lower  $\Psi_l$  values beyond the shown linear trend in Fig. 9). Additionally, the supply functions for DaS 322–327 (filled circles in Fig. 9) might have been flatter than those for the previous days, since vpd remained high and the soil had dried out significantly (Fig. 2b and f) after the stomatal closure on DaS 319.

The fact that the simultaneous drop of  $G_s$  and Tr occurred a few days before the relationship between

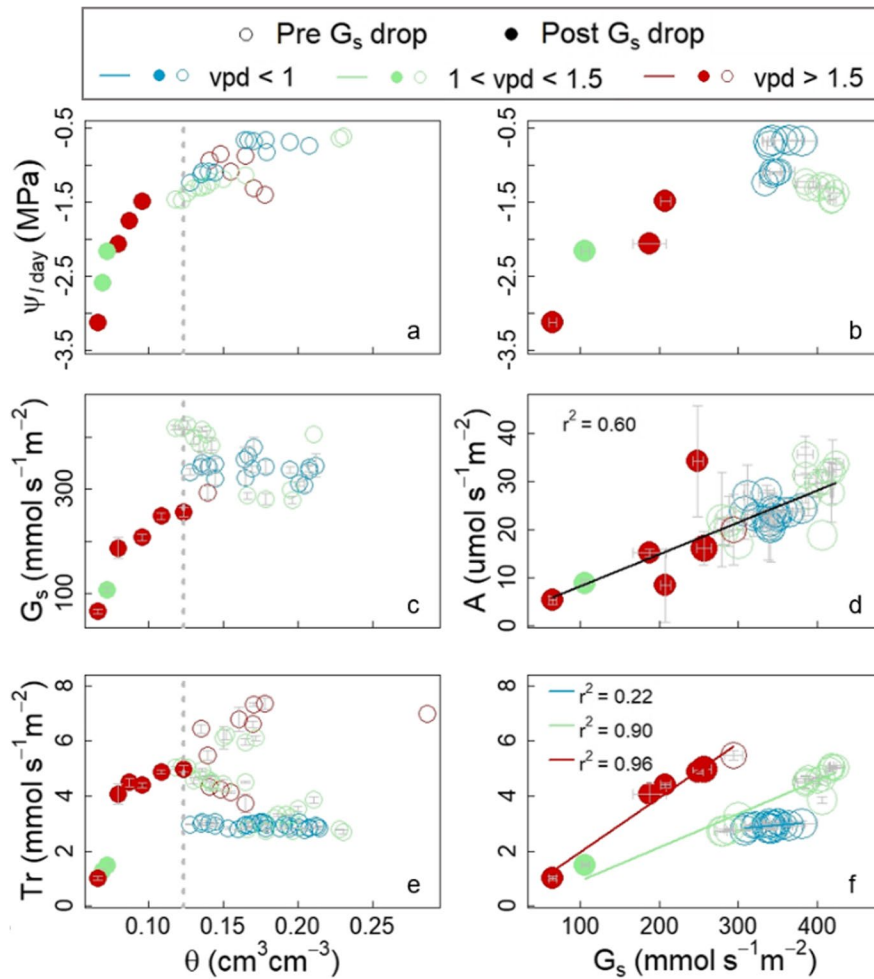


**Fig. 8** Minimum leaf water potential during day (light panel on) ( $\Psi_{l\text{-day}}$ , MPa), canopy conductance ( $G_s$ ,  $\text{mmol s}^{-1} \text{m}^{-2}$ ) and transpiration rate ( $\text{Tr}$ ,  $\text{mmol s}^{-1} \text{m}^{-2}$ ) as a function of soil water content ( $\theta$ ,  $\text{cm}^3 \text{cm}^{-3}$ ) (a, c and e, respectively).  $\Psi_{l\text{-day}}$ ,  $\text{CO}_2$  assimilation rate ( $A$ ,  $\mu\text{mol s}^{-1} \text{m}^{-2}$ ) and  $\text{Tr}$  as a function of  $G_s$  (b, d and f, respectively). The correlations in panels d and f were significant (i.e.,  $p\text{-value} < 0.05$ ). The dashed gray line in panels a, c and e marks the soil water content value ( $\theta$ ,  $\text{cm}^3 \text{cm}^{-3}$ ) on day after seeding (DaS) 319, when canopy

conductance started dropping steadily to zero. Empty circles represent days before this drop (pre  $G_s$  drop) and filled circles represent days after DaS 319 (post  $G_s$  drop). The color of the symbols represents vapor pressure deficit (vpd, kPa): blue for days with vpd below 1 kPa, green for days with vpd between 1 and 1.5 kPa, and red for days with vpd higher than 1.5 kPa. In panels b, d and f, the symbol size represents the mean  $\theta$  along the isotopic column (i.e., the bigger the circle, the higher the  $\theta$  value in that day)

$\text{Tr}$  and  $\Psi_l$  deviated from a relatively linear trend observed until DaS 321 (empty circles in Fig. 9) further supports our assumption of stomatal closure as a strategy to avoid hydraulic failure. Hayat et al. (2020) also observed a concomitant reduction in soil-canopy conductance, stomatal conductance and  $\text{Tr}$  in maize plants when the soil was drying. They also argued that reducing  $\text{Tr}$  through

stomatal closure following a reduction in soil-canopy conductance is an attempt to avoid what they call “non-linearities” in the  $\text{Tr}(P_{\text{canopy}})$  relationship (i.e., approaching the critical  $\text{Tr}$  value). Investigating the temporal and spatial dynamics of the soil-canopy conductance and of hydraulic characteristics at the root-soil interface during our experiment (as done by Rodriguez-Dominguez and Brodrribb 2020;

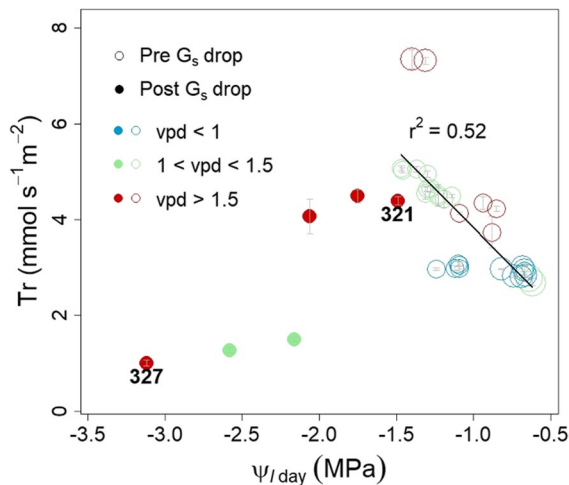


**Fig. 9** Plant transpiration rate ( $Tr$ ,  $\text{mmol s}^{-1} \text{m}^{-2}$ ) as a function of minimum leaf water potential during day (light panel on) ( $\Psi_{l\text{-day}}$ , MPa). The correlation is significant (i.e.,  $p\text{-value} < 0.05$ ). Empty circles represent days before day after seeding (DaS) 319, when canopy conductance started dropping steadily to zero (pre  $G_s$  drop). The filled circles represent days after DaS 319 (post  $G_s$  drop). The numbers next to two of the filled red circles are the DaS of the observation point. The color of the symbols represents vapor pressure deficit (vpd, kPa): blue for days with vpd below 1 kPa, green for days with vpd between 1 and 1.5 kPa, and red for days with vpd higher than 1.5 kPa. The symbol size represents the mean soil water content ( $\theta$ ,  $\text{cm}^3 \text{cm}^{-3}$ ) along the isotopic column (i.e., the bigger the circle, the higher the  $\theta$  value in that day)

Sperry et al. 2002 and as suggested by Carminati and Javaux 2020) would have helped further substantiate our assumptions.

Moreover, reductions in soil-canopy conductance (followed by reductions in stomatal conductance and  $Tr$ ) reported by Hayat et al. (2020) started at relatively high  $\theta$  values ( $0.12 \text{ cm}^3 \text{cm}^{-3}$ ). In our study,  $\theta$  was relatively high (around  $0.12 \text{ cm}^3 \text{cm}^{-3}$ ) when  $G_s$ ,  $Tr$  and  $A$ , started decreasing on DaS 319 (Fig. 1b and d, f).  $\Psi_l$  was around  $-1.5$  MPa at this point, a value observed on other DaS with higher  $\theta$  and  $G_s$  values (empty circles in Fig. 8a and b). The results of Hayat et al. (2020) and our own potentially agree with the hypothesis of Gollan et al. (1985) that leaf gas exchange might be limited when a critical value of  $\theta$  (alternatively, a critical value of soil water potential) is reached rather than when a critical leaf water potential is exceeded. Leaf gas exchange in the last days of the experiment was limited by both a drying soil and increasingly negative  $\Psi_l$  values:  $G_s$  values

decreased steadily with decreasing  $\Psi_l$  values after DaS 319, while no trend was observed before this day (Fig. 8b).

#### Iso- or anisohydricity

Similar to Kübert et al. (2021), we observed that *C. jacea* could maintain relatively high  $Tr$  in dry soils and at high vpd by withstanding very low  $\Psi_l$  values (Fig. 7). This pointed towards an anisohydric behavior. However, a deeper analysis of the  $\Psi_l$  values during the experiment revealed that this conclusion might be incomplete.

The correlation between  $\Psi_{l\text{-day}}$  (i.e., minimum  $\Psi_l$  while the LED panel was on) and  $\Psi_{l\text{-night}}$  (i.e., maximum  $\Psi_l$  while the LED panel was off) was below 1 (slope = 0.89,  $r^2 = 0.86$ ,  $p\text{-value} = 2.2 \times 10^{-16}$ ) during the experiment, indicating an isohydric behavior (Martínez-Vilalta et al. 2014; Zhao et al. 2021). However, when considering the data before DaS 321 when  $\theta$  dropped below  $\sim 0.10 \text{ cm}^3 \text{cm}^{-3}$  only, the computed slope is above 1 (slope = 1.78,  $r^2 = 0.58$ ,  $p\text{-value} = 2.8 \times 10^{-9}$ ), pointing to an anisohydric behavior. Furthermore, the variation in  $\Delta\Psi_l = \Psi_{l\text{-day}} - \Psi_{l\text{-night}}$  was comparable to the variation observed in the anisohydric plant in the study of Zhao et al. (2021) ( $\sim 0.40$  MPa). Though, the median  $\Delta\Psi_l$  in our experiment ( $-0.47$  MPa) was closer to the value calculated for the isohydric plant ( $\sim -0.77$  MPa) of the same study (the value for the anisohydric plant was  $\sim -1.70$  MPa). Also, there was no significant correlation between  $G_s$  and  $\Psi_{l\text{-day}}$  (Fig. 8b), another characteristic of anisohydric behavior according to Zhao et al. (2021), and  $\Psi_l$  steadily dropped when  $\theta$  decreased (see period HTr-II in Fig. 1c), also pointing towards anisohydricity.

The analysis presented in the last paragraph supports the idea that isohydric and anisohydric behavior should be viewed as a more or less continuous spectrum rather than a dichotomy (Martínez-Vilalta et al. 2014) and that it is possible for a species to display both behaviors. Alternatively, there have been recent calls to abandon the iso- and anisohydricity terms and instead assess plant performance during drought through parameters such as maximum transpiration rate, hydraulic conductance and critical leaf water potential (Hochberg et al. 2018). According to Hochberg et al. (2018), by using these parameters, the

effect of environmental factors could be eliminated when comparing the response of plant species or genotypes to drought.

### RWU dynamics and drivers

In the following paragraphs we (i) describe the role of root distribution (i.e., root length density or RLD) in root water uptake (RWU), (ii) the impact of above- and below-ground dry conditions on RWU, and (iii) water movement processes through the soil and the roots observed in our experiment.

#### *RLD monitoring and its role in RWU*

Using MRI to monitor root distribution and growth requires careful selection and preparation of the soil (e.g., removal of ferromagnetic particles), and characteristics of the pot (a bigger diameter decreases the signal-to-noise ratio of the images, and thus thin roots are not visible). By comparing root mass and length obtained from MRI and from destructive sampling (e.g., root extraction and scanning) using a particular soil, plant and pot size, we can determine a root-diameter threshold (van Dusschoten et al. 2016), differences in root diameter in the soil profile and we can correct  $\theta$  measurements (van Dusschoten et al. 2020). The ten-fold difference between the MRI- and scan-derived RLD profiles could primarily stem from the fact that the average root diameter along the isotopic column was  $0.36 \pm 0.04$  mm, right above the lower detection limit of MRI with the used coil and measurement settings ( $\sim 0.3$  mm). Beyond these differences and limitations, the RLD profiles from the MRI analysis agreed well with those obtained with WinRhizo<sup>TM</sup>. This fact highlights the potential of MRI to monitor at a much higher temporal resolution (e.g., daily) and with a higher repeatability root development in the same plant individual.

In some studies, root distribution and RWU profiles are rather similar (e.g., for grass species in Mazzacavallo and Kulmatiski 2015), whereas in other studies there is no clear and consistent association (e.g., Kühnhammer et al. 2020). In our study, RWU at the bottom of the isotopic column (45–60 cm) was consistently lower than RWU at the top (0–15 cm), even if the percentage of total

root length and root volume in the same soil layers was comparable. On DaS 307, 33.9% and 31.5% of the total root length and volume, respectively, were located in the soil layer 0–15 cm, whereas 37.9% and 39.2% of the total root length and volume, respectively, were located in the soil layer 45–60 cm. On DaS 327, the soil layer 0–15 cm contained 34.8% and 39.4% of the total root length and volume, respectively, whereas the soil layer 45–60 cm contained 35.8% and 32.9% of the total root length and volume, respectively. Our observations, like the results of Kulmatiski et al. (2010) regarding the overestimation of root activity from root mass, potentially confirms the conclusion drawn by Schenk (2008): most plants will develop the “shallowest possible” root and water extraction profile. This fits our observation that RWU from *C. jacea* was highest in layer 0–15 cm under varying hydro-climatic conditions. However, since we could not quantify root-mediated soil water redistribution (i.e., hydraulic lift) with our isotope-based methodology, we do not entirely rule out a potential underestimation of water extraction by deep roots (see [Redistribution of water in the soil](#) section).

#### *RWU dynamics under varying above- and below-ground environmental conditions*

The comparison made between the  $\delta^2\text{H}$ - $\delta^{18}\text{O}$ -,  $\delta^2\text{H}$ - and  $\delta^{18}\text{O}$ -derived RWU profiles assisted us in assessing potential isotope-specific ( $^2\text{H}$  or  $^{18}\text{O}$ ) fractionation during root water uptake or artifacts during the non-destructive sampling of soil water vapor and plant chamber water vapor. We did not observe neither isotope-specific fractionation during RWU nor methodological artifacts, since no statistically significant differences between RWU profiles were generally found, to the single exception of DaS 245 between  $\delta^2\text{H}$ - and  $\delta^2\text{H}$ - $\delta^{18}\text{O}$ -derived RWU profiles. This is why we will only discuss the dynamics of  $\delta^2\text{H}$ - $\delta^{18}\text{O}$ -derived RWU profiles in this section.

The calculated RWU profiles in periods with high and low Tr were very similar in well-watered and dry conditions: up to 79% of RWU happened in the soil layer 0–15 cm and up to 44% of RWU happened in the soil layer 45–60 cm (see [Daily RWU profiles](#) section). Hayat et al. (2019) also

obtained similar relative RWU profiles from maize under uniform  $\theta$  conditions when Tr was high and low. However, the RWU in their study shifted (i.e., was higher) to deeper wetter soil layers in non-uniform  $\theta$  conditions. The investigation conducted by Warren (2011) also shows evidence of this RWU shift in *Centaurea diffusa* towards deeper soil layers when the shallow ones had dried out. There are numerous studies reporting higher water extraction from deeper wetter soil layers by trees (e.g., Ehleringer and Dawson 1992; Volkman et al. 2016). Nonetheless, there are some studies that reported no such shift in some tree species during drought (e.g., Gessler et al. 2022). In the case of grassland species, it has been observed that some still extract water from the top soil, even if  $\theta$  is approaching permanent wilting point (Kulmatiski et al. 2010; Bachmann et al. 2015; Prechsl et al. 2015). Kühnhammer et al. (2020) proposed that significant RWU by *C. jacea* from shallow soil layers, even if water is available deeper in the soil profile, might be a strategy for maximizing the use of rainwater, especially when drought conditions prevail. Even if we did not observe a marked shift in RWU to wetter deeper layers (i.e., highest RWU values in layers with the highest  $\theta$  values), we did observe an increase of RWU in wetter deeper layers when the soil layer 0–15 cm was drying out and when transpiration rate was high.

Not only water availability, root distribution (see [RLD monitoring and its role in RWU](#) section) and environmental factors (i.e., vpd or light intensity) were driving RWU, but also nutrient availability might have played a significant role in our experiment (Kulmatiski et al. 2017). Nutrients in irrigation water were added at the top and the bottom of the column before the isotopic labeling started, and most probably, the amount of irrigation water was not sufficient to reach the middle section of the column and a gradient in nutrient content along the column was established. Alternatively, the addition of water for about 57 days on a daily basis from the top and the bottom in relatively small amounts could have been a driver of RWU of *C. jacea*, since  $\theta$  was locally and temporally very high at the top and at the bottom (Fig. 6d). A better strategy would probably be to add smaller amounts of water with a much higher  $\delta$ -value for a shorter period at

different depths, so that the changes in  $\theta$  are homogeneous along the soil column and, to some extent, negligible.

#### *Redistribution of water in the soil*

Mismatches between  $\theta$  and RWU profiles, like the ones described in other studies and in “[Daily RWU profiles](#)” section, are to be expected, since changes in  $\theta$  are not only due to RWU, but also to soil water redistribution (Zarebanadkouki et al. 2013). This redistribution can happen through capillary forces or even through hydraulic lift (Meunier et al. 2017; Couvreur et al. 2020). Kühnhammer et al. (2020) described such mismatches in an experimental setup comparable to ours. For example, for some periods they observed daily changes in  $\theta$  greater than daily changes in estimated RWU in depth 30–60 cm and almost no changes in  $\theta$  in depth 1 cm, even though RWU there was high.

Soil water redistribution could also be the reason why the isotopic profile in layer 0–10 cm became progressively non-monotonic from DaS 318 onwards (Fig. 3d). Contrary to our observations, water diffusion promoted solely by the isotopic and soil water content gradients would have resulted in a gradual and homogeneous shift of the entire isotopic profile towards the middle. That is, the changes in the isotopic profile in the soil layer 0–30 cm would have been similar to those in the isotopic profile in the soil layer 30–60 cm. In a scenario where hydraulic lift took place, water extracted by the roots from the deepest soil layers (i.e., 55–60 cm characterized by a higher soil water potential, Fig. 7d) could have been released locally in soil layer 0–10 cm. This would have resulted in a greater increase of  $\delta^2\text{H}$  and a greater decrease of  $\delta^{18}\text{O}$  from day to day in soil layer 0–10 cm than in layer 10–55 cm. Such changes in the isotopic profile are observed in Fig. 3d, which could be evidence of hydraulic lift. In this case, calculation of the sink term using transpiration rate and soil water isotopic composition may lead to an underestimation of water uptake from the roots at the bottom of the column, since water extracted by these roots might have been released at the top and later taken up by the shallow roots. However, process-based modeling (i.e., where hydraulic redistribution by roots

can be simulated) is necessary to test the validity of this hypothesis (Rothfuss and Javaux 2017), that is, distinguish between soil- and root-mediated water redistribution.

## Conclusion

In the present study, we were able to obtain root water uptake (RWU) profiles of *Centaurea jacea* with daily and centimeter resolution, and to assess the ability of this plant to acclimate to challenging environmental conditions. The coupling between an automated experimental system and the latest soil and plant water isotopic monitoring and root imaging techniques allowed for a fully non-destructive approach. The control of gas exchange at the leaf level in response to drought was proven mostly anisohydric, although at other moments during our experiment stomatal control could be described as isohydric. Under dry conditions, leaf water potential in this plant species reached low values, which allowed *C. jacea* to maintain high transpiration rates and relatively constant intrinsic water use efficiency values without causing hydraulic disruption in the soil-plant-atmosphere continuum. However, we also observed a decline in canopy conductance that potentially limited transpiration and carbon assimilation rates before leaf water potential and soil water content markedly decreased. Under well-watered conditions, transpiration rate was mainly driven by vapor pressure deficit and light intensity.

Under laboratory conditions, up to 79% of RWU by *C. jacea* occurred in shallow depths and up to 44% of RWU, in deeper soil layers. We were able to explain the adaptation of RWU patterns with both root distribution and water availability profiles. Even though *C. jacea* displayed effective adaptation strategies to a dry environment, its apparent and consistent reliance on water in shallow soil depths could negatively affect the performance and competitiveness of this species in a future climate, projected to be associated with more frequent and prolonged drought

periods. Nevertheless, the significance of the activity of deep roots in the adaptation of *C. jacea* to dry conditions might have been underestimated, since we only quantified root water extraction for plant transpiration, but not soil water redistribution through the roots.

## Appendix 1 Calculation of the relative contribution of soil water to plant transpiration profiles in SIAR

We ran the function *siarmcmmdirichletv4* 1,000 times for each day from DaS 270 to 312. The number of iterations and values for burn-in and thinning in each of the runs were set at 500,000, 50,000 and 15, respectively. That is, in each run, 30,000 iterations out of 500,000 were considered for calculating the vector of most frequent relative contribution value for each depth (i.e., mfv). Since the mfv vector did not add up to one as each and one of the iterations did, the iteration (i.e., “best iteration”) with the “greatest probability of occurrence” (as defined by Couvreur et al. 2020) was identified. The “best iteration” (or *bi*) was the vector of relative contribution values with the lowest root mean square error (RMSE) when compared with the mfv vector. That is, the *bi* minimized the following objective function (OF) in Eq. (A1) (Couvreur et al. 2020)

$$OF = \sqrt{\frac{\sum_{j=1}^{11} (mfv_j - bi_j)^2}{11}} \quad (A1)$$

The aforementioned process was performed 1,000 times and a “best run” out of the 1,000 “best iterations” was identified. A new mfv vector from the 1,000 “best iterations” was calculated and the vector of relative contribution values for a particular day was identified as the one with the lowest RMSE when compared with this new mfv vector.

## Appendix 2

Table 2

**Table 2** List of abbreviations and symbols

Abbreviations and symbols	Description	Unit / Dimension
A	CO <sub>2</sub> assimilation rate	μmol s <sup>-1</sup> m <sup>-2</sup>
c <sub>in</sub>	CO <sub>2</sub> mixing ratio of the water vapor in the inlet airstream	-
c <sub>out</sub>	CO <sub>2</sub> mixing ratio of the water vapor in the outlet airstream	-
CRDS	Cavity ring-down spectrometer	-
DaS	Days after seeding	-
G <sub>s</sub>	Canopy conductance	mmol s <sup>-1</sup> m <sup>-2</sup>
HTr	High transpiration rate	-
IRIS	Isotope Ratio Infrared Spectrometer	-
iWUE	Intrinsic water use efficiency	μmol mmol <sup>-1</sup>
LED	Light-emitting diode	-
LTr	Low transpiration rate	-
L <sub>z</sub>	Thickness of soil layer z	cm
MRI	Magnetic resonance imaging	-
MS	Multi-source	-
P <sub>air</sub>	Vapor saturation pressure at air temperature	kPa
P <sub>canopy</sub>	Canopy xylem pressure	P
P <sub>leaf</sub>	Vapor saturation pressure at leaf temperature	kPa
ppmV	parts per million volume	-
PVC	Polyvinyl chloride	-
rh	Air relative humidity	%
rh'	Relative humidity normalized to leaf temperature	%
RLD	Root length density	-
RL <sub>z</sub>	Total root length in soil layer z	cm
rRLD	Relative root length density	-
RWU	Root water uptake	-
s	Soil surface area of the column	m <sup>2</sup>
SIAR	Stable Isotope Analysis with R	-
SWaP	Soil water profiler	-
T <sub>air</sub>	Air temperature	°C
T <sub>leaf</sub>	Leaf temperature	°C
Tr	Plant transpiration rate	mmol s <sup>-1</sup> m <sup>-2</sup>
u <sub>in</sub>	Molar air flow into the plant chamber	mmol s <sup>-1</sup>
vpd	Vapor pressure deficit	kPa
vpd <sub>l</sub>	Air-to-leaf vapor pressure deficit	kPa
V-SMOW	Vienna standard mean ocean water	-
V <sub>z</sub>	Soil volume of layer z	cm <sup>3</sup>
w <sub>in</sub>	Mixing ratio of the water vapor in the inlet airstream	-
w <sub>out</sub>	Mixing ratio of the water vapor in the outlet airstream	-
WUE	Instantaneous water use efficiency	μmol mmol <sup>-1</sup>
δ <sub>Tr</sub>	Isotopic composition of plant transpiration	‰
δ <sub>soil water</sub>	Isotopic composition of soil water	‰
θ	Volumetric soil water content	cm <sup>3</sup> cm <sup>-3</sup>
Ψ <sub>l</sub>	Leaf water potential	MPa

**Acknowledgements** The authors would like to thank Andreas Lücke, Lutz Weihermüller, Holger Wissel, Beate Uhlig, Marco Dautzenberg, Johannes Kochs, Daniel Pflugfelder, Sandi Moyo, Helena Jorda, Normen Hermes and Moritz Harings for their scientific and technical support.

**Author contributions** YR, MD, DvD, MJ, SM, NB and PDD planned and designed the experiment. DvD, YR and PDD conducted the experiment. DvD and PDD collected the laboratory data. AK, MD, YR and PDD analysed the data. AK, DvD, MD, NB, JV and YR helped with data interpretation. PDD wrote the manuscript and all authors reviewed and improved the manuscript.

**Funding** Open Access funding enabled and organized by Projekt DEAL. The present work was conducted within the framework of the DFG-funded research programme ‘Assessing ecohydrological responses from single plant to community scale using a stable isotope approach’ (RO-5421/1–1 and DU-1688/1–1). Additional funding was provided by the project ‘Combining Root contrasted Phenotypes for more resilient agro-ecosystem’ (CROP; <https://www.bonares.de/crop>).

**Data availability** Upon acceptance, all of the research data that were required to create the plots will be available from reliable FAIR-aligned data repositories with assigned DOIs. The data is also available upon request.

#### Declarations

**Competing interests** The authors declare that they have no conflict of interest.

**Open Access** This article is licensed under a Creative Commons Attribution 4.0 International License, which permits use, sharing, adaptation, distribution and reproduction in any medium or format, as long as you give appropriate credit to the original author(s) and the source, provide a link to the Creative Commons licence, and indicate if changes were made. The images or other third party material in this article are included in the article’s Creative Commons licence, unless indicated otherwise in a credit line to the material. If material is not included in the article’s Creative Commons licence and your intended use is not permitted by statutory regulation or exceeds the permitted use, you will need to obtain permission directly from the copyright holder. To view a copy of this licence, visit <http://creativecommons.org/licenses/by/4.0/>.

#### References

- Bachmann D et al (2015) No evidence of complementary water use along a plant species richness gradient in temperate experimental grasslands. *PLoS ONE* 10(1):1–14. <https://doi.org/10.1371/journal.pone.0116367>
- Beyer M et al (2018) Examination of deep root water uptake using anomalies of soil water stable isotopes, depth-controlled isotopic labeling and mixing models. *J Hydrol* 566:122–136. Elsevier. <https://doi.org/10.1016/j.jhydrol.2018.08.060>
- Bogena HR et al (2007) Evaluation of a low-cost soil water content sensor for wireless network applications. *J Hydrol* 344(1–2):32–42. <https://doi.org/10.1016/j.jhydrol.2007.06.032>
- Carminati A, Javaux M (2020) Soil rather than Xylem vulnerability controls stomatal response to drought. *Trends Plant Sci*, The Authors 25(9):868–880. <https://doi.org/10.1016/j.tplants.2020.04.003>
- Chitra-Tarak R et al (2021) Hydraulically-vulnerable trees survive on deep-water access during droughts in a tropical forest. *New Phytol* 231(5):1798–1813. <https://doi.org/10.1111/nph.17464>
- Couvreur V et al (2020) Disentangling temporal and population variability in plant root water uptake from stable isotopic analysis: when rooting depth matters in labeling studies. *Hydrol Earth Syst Sci* 24(6):3057–3075. <https://doi.org/10.5194/hess-24-3057-2020>
- Cowan IR, Farquhar GD (1977) Stomatal function in relation to leaf metabolism and environment: Stomatal function in the regulation of gas exchange. University Press, Cambridge, pp 471–505
- Dubbett M, Cuntz M et al (2014) Oxygen isotope signatures of transpired water vapor: The role of isotopic non-steady-state transpiration under natural conditions. *New Phytol* 203(4):1242–1252. <https://doi.org/10.1111/nph.12878>
- Dubbett M, Piayda A et al (2014) Stable oxygen isotope and flux partitioning demonstrates understory of an oak savanna contributes up to half of ecosystem carbon and water exchange. *Front Plant Sci* 5:1–17. <https://doi.org/10.3389/fpls.2014.00530>
- Ehleringer JR, Dawson TE (1992) Water uptake by plants: perspectives from stable isotope composition. *Plant Cell Environ* 15(9):1073–1082. <https://doi.org/10.1111/j.1365-3040.1992.tb01657.x>
- Gang C et al (2016) Drought-induced dynamics of carbon and water use efficiency of global grassland from 200 to 2011. *Ecol Indic* 67:788–797
- Gessler A et al (2022) Drought reduces water uptake in beech from the drying topsoil, but no compensatory uptake occurs from deeper soil layers. *New Phytol* 233(1):194–206. <https://doi.org/10.1111/nph.17767>
- Gollan T, Turner NC, Schulze ED (1985) The responses of stomata and leaf gas exchange to vapour pressure deficits and soil water content. *Oecologia* 65:356–362
- Hayat F et al (2019) Measurements and simulation of leaf xylem water potential and root water uptake in heterogeneous soil water contents. *Adv Water Resour* 124:96–105

- Hayat F et al (2020) Transpiration reduction in maize (*Zea mays* L) in response to soil drying. *Front Plant Sci* 10(January):1–8. <https://doi.org/10.3389/fpls.2019.01695>
- Hegi G (1954) Dicotyledones. *Illustrierte Flora von Mitteleuropa. Mit besonderer Berücksichtigung von Oesterreich, Deutschland und der Schweiz. Zum Gebrauche in den Schulen und zum Selbstunterricht, Volume VI. 2nd Part.* Omnitypie-Gesellschaft, Stuttgart
- Hochberg U et al (2018) Iso / Anisohydry: A plant – Environment interaction rather than a simple hydraulic trait. *Trends Plant Sci* 23:112–120. 2. Elsevier Ltd. <https://doi.org/10.1016/j.tplants.2017.11.002>.
- Jentsch A et al (2011) Climate extremes initiate ecosystem-regulating functions while maintaining productivity. *J Ecol* 99:689–702. <https://doi.org/10.1111/j.1365-2745.2011.01817.x>
- Judson PH et al (2006) Advantages in water relations contribute to greater photosynthesis in *Centaurea maculosa* compared with established grasses. *Int J Plant Sci* 167(2):269–277
- Kübert A et al (2021) Combined experimental drought and nitrogen loading: the role of species-dependent leaf level control of carbon and water exchange in a temperate grassland. *Plant Biol* 23(3):427–437. <https://doi.org/10.1111/plb.13230>
- Kühnhammer K et al (2020) Investigating the root plasticity response of *Centaurea jacea* to soil water availability changes from isotopic analysis. *New Phytol* 226(1):98–110. <https://doi.org/10.1111/nph.16352>
- Kulmatiski A et al (2010) A depth-controlled tracer technique measures vertical, horizontal and temporal patterns of water use by trees and grasses in a subtropical savanna. *New Phytol* 188(1):199–209. <https://doi.org/10.1111/j.1469-8137.2010.03338.x>
- Kulmatiski A et al (2017) Water and nitrogen uptake are better associated with resource availability than root biomass. *Ecosphere* 8(3). <https://doi.org/10.1002/ecs2.1738>
- Majoube M (1971) Fractionnement en oxygène 18 et en deutérium entre l'eau et sa vapeur. *J Chem Phys* 68:1423–1436
- Martínez-Vilalta J et al (2014) A new look at water transport regulation in plants. *New Phytol* 204(1):105–115. <https://doi.org/10.1111/nph.12912>
- Maseda PH, Fernández RJ (2006) Stay wet or else: Three ways in which plants can adjust hydraulically to their environment. *J Exp Bot* 57(15):3963–3977. <https://doi.org/10.1093/jxb/erl127>
- Mazzacavallo MG, Kulmatiski A (2015) Modelling water uptake provides a new perspective on grass and tree coexistence. *PLoS ONE* 10(12):1–16. <https://doi.org/10.1371/journal.pone.0144300>
- Meunier F et al (2017) Measuring and modeling hydraulic lift of *Lolium multiflorum* using stable water isotopes. *Vadose Zone J* 17(1):160134. <https://doi.org/10.2136/vzj2016.12.0134>
- Murray FW (1966) On the computation of saturation vapor pressure. (No. P-3423). Rand Corp, Santa Monica. <https://www.rand.org/pubs/papers/P3423.html>
- Newman BD et al (2006) Ecohydrology of water-limited environments: A scientific vision. *Water Resour Res* 42:1–15. <https://doi.org/10.1029/2005WR004141>
- Parnell AC et al (2010) Source partitioning using stable isotopes: Coping with too much variation. *PLoS ONE* 5(3):1–5. <https://doi.org/10.1371/journal.pone.0009672>
- Pflugfelder D et al (2017) Non-invasive imaging of plant roots in different soils using magnetic resonance imaging (MRI). *Plant Methods* 13(1):1–9. BioMed Central. <https://doi.org/10.1186/s13007-017-0252-9>
- Prechsl UE et al (2015) No shift to a deeper water uptake depth in response to summer drought of two lowland and sub-alpine C3-grasslands in Switzerland. *Oecologia* 177(1):97–111. <https://doi.org/10.1007/s00442-014-3092-6>
- Quade M et al (2018) Investigation of kinetic isotopic fractionation of water during bare soil evaporation. *Water Resour Res* 54:6909–6928. <https://doi.org/10.1029/2018WR023159>
- R Core Team (2020) R: A language and environment for statistical computing. R Foundation for Statistical Computing, Vienna. <https://www.R-project.org/>
- Rodríguez-Domínguez CM, Brodribb TJ (2020) Declining root water transport drives stomatal closure in olive under moderate water stress. *New Phytol* 225(1):126–134. <https://doi.org/10.1111/nph.16177>
- Rothfuss Y et al (2015) Long-term and high-frequency non-destructive monitoring of water stable isotope profiles in an evaporating soil column. *Hydrol Earth Syst Sci* 12:3893–3918. <https://doi.org/10.5194/hess-19-4067-2015>
- Rothfuss Y, Javaux M (2017) Reviews and syntheses: Isotopic approaches to quantify root water uptake: A review and comparison of methods. *Biogeosciences* 14:2199–2224. <https://doi.org/10.5194/bg-14-2199-2017>
- Rothfuss Y, Vereecken H, Brüggemann N (2013) Monitoring water stable isotopic composition in soils using gas-permeable tubing and infrared laser absorption spectroscopy. *Water Resour Res* 49:3747–3755. <https://doi.org/10.1002/wrcr.20311>
- Schenk HJ (2008) The shallowest possible water extraction profile: a null model for global root distributions. *Vadose Zone Journal* 7(3):1119–1124. <https://doi.org/10.2136/vzj2007.0119>
- Sperry JS et al (2002) Water deficits and hydraulic limits to leaf water supply. *Plant Cell Environ* 25(2):251–263. <https://doi.org/10.1046/j.0016-8025.2001.00799.x>
- Sperry JS, Love DM (2015) What plant hydraulics can tell us about responses to climate-change droughts. *New Phytol* 207(1):14–27. <https://doi.org/10.1111/nph.13354>
- Tardieu F, Simonneau T (1998) Variability among species of stomatal control under fluctuating soil water status and evaporative demand: modelling isohydric and anisohydric behaviours. *J Exp Bot* 49:419–432
- van Dusschoten D et al (2016) Quantitative 3D analysis of plant roots growing in soil using magnetic resonance imaging. *Plant Physiol* 170(3):1176–1188. <https://doi.org/10.1104/pp.15.01388>

- van Dusschoten D et al (2020) Spatially resolved root water uptake determination using a precise soil water sensor. *Plant Physiol* 184(3):1221–1235. <https://doi.org/10.1104/pp.20.00488>
- von Caemmerer S, Farquhar GD (1981) Some relationships between the biochemistry of photosynthesis and the gas exchange of leaves. *Planta* 153(4):376–387. <https://doi.org/10.1007/BF00384257>
- Volkman THM et al (2016) High-resolution isotope measurements resolve rapid ecohydrological dynamics at the soil-plant interface. *New Phytol* 210(3):839–849. <https://doi.org/10.1111/nph.13868>
- Warren CP (2011) Isotopic tracer reveals depth-specific water use patterns between two adjacent native and non-native plant communities. Utah State University
- Yang Y et al (2016) Contrasting responses of water use efficiency to drought across global terrestrial ecosystems. *Sci Rep* 6:1–8. Nature Publishing Group. <https://doi.org/10.1038/srep23284>.
- Yue P et al (2020) Biometeorological effects on carbon dioxide and water-use efficiency within a semiarid grassland in the Chinese Loess Plateau. *J Hydrol* 590:125520. Elsevier. <https://doi.org/10.1016/j.jhydrol.2020.125520>
- Zarebanadkouki M, Kim YX, Carminati A (2013) Where do roots take up water? Neutron radiography of water flow into the roots of transpiring plants growing in soil. *New Phytol* 199(4):1034–1044. <https://doi.org/10.1111/nph.12330>
- Zhao Y et al (2021) Contrasting adaptive strategies by *Caragana korshinskii* and *Salix psammophila* in a semiarid revegetated ecosystem. *Agric For Meteorol* 300:108323. Elsevier B.V. <https://doi.org/10.1016/j.agrfor.2021.108323>
- Zwicke M et al (2015) What functional strategies drive drought survival and recovery of perennial species from upland grassland? *Ann Bot* 116(6):1001–1015. <https://doi.org/10.1093/aob/mcv037>

**Publisher's note** Springer Nature remains neutral with regard to jurisdictional claims in published maps and institutional affiliations.